

# Single-Particle Photoluminescence Measures a Heterogenous Distribution of Differential Circular Absorbance of Gold Nanoparticle Aggregates near Constricted Thioflavin T Molecules

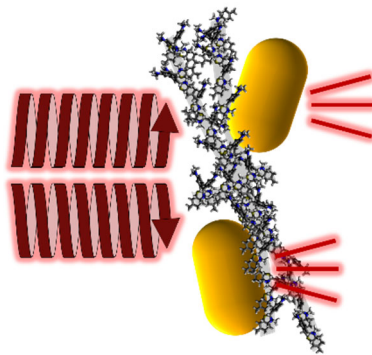
Saaj Chattopadhyay<sup>1</sup>, Maciej Lipok<sup>2</sup>, Zechariah J. Pfaffenberger<sup>3</sup>, Joanna Olesiak-Bańska<sup>2</sup>, Julie S. Biteen<sup>1,3\*</sup>

<sup>1</sup>Applied Physics Program, University of Michigan, Ann Arbor, MI 48104 USA

<sup>2</sup>Institute of Advanced Materials, Wroclaw University of Science and Technology, 50-37044 Wroclaw Poland

<sup>3</sup>Department of Chemistry, University of Michigan, Ann Arbor, MI 48104 USA

\*Correspondence to: [jsbiteen@umich.edu](mailto:jsbiteen@umich.edu)



## Abstract:

The chirality of biomacromolecules is critical for their function, but the optical signal of this chirality is small in the visible range. Plasmonic nanoparticles are antennas that can couple to this chiral signal. Here, we examine the molecular-scale mechanism behind the induced circular dichroism of gold nanorods (AuNRs) in a solution with insulin fibrils and the fibril-intercalating dye thioflavin T (ThT) with polarization-resolved single-molecule fluorescence and single-particle photoluminescence (PL) imaging. We compared the PL upon excitation by left- and right-handed circularly polarized light to calculate the differential absorbance of AuNRs near insulin fibrils with and without ThT. Overall, our results indicate that AuNRs do not act as chiral absorbers near constricted ThT molecules. Instead, we hypothesize that fibrils promote AuNR aggregation, and this templating is mediated by subtle changes in the solution conditions; under the right conditions, only a few chiral aggregates with significantly higher circular dichroism signal contribute to a large net circular dichroism.

## Main

Amyloid fibrils are protein assemblies that often cannot be superimposed onto their mirror image<sup>1</sup>. This signature handedness, or chirality, correlates with their biological function<sup>2</sup>. If fibril formation is disrupted or the fibrils are damaged, the fibril chirality is affected<sup>3–6</sup>. Thus, sensitive detection of a fibril's chirality could improve the early diagnosis of plaque-related diseases<sup>7–9</sup>. Fibril chirality can be measured with circular dichroism<sup>10</sup>. This measurement typically requires high concentrations (~100  $\mu$ M) and large enough volumes (~1 mL) for enough signal. A recent study has also shown that plasmonic nanoparticles that match the fibril pitch form ordered structures around the fibril, which can be used to detect fibril chirality at low concentrations<sup>11</sup>. Plasmonic nanoparticles can also amplify the resonant chiroptical signal by plasmon-coupled circular dichroism<sup>12</sup>. Here, we probe if 80 nm  $\times$  40 nm gold nanorods (AuNRs) that are strong enough scatterers for detection in single-particle photoluminescence (PL) microscopy and dark-field scattering spectroscopy, but much larger than the fibril pitch, can also be used as a sensitive detector for fibril chirality upon addition of the fibril-binding dye thioflavin T (ThT). We used insulin fibrils as our model fibril system and selected ThT because it acts as a fluorescent probe and a chiral molecule upon binding to the fibrils<sup>13,14</sup>. The 80 nm  $\times$  40 nm AuNRs have a strong plasmon resonance near 640 nm (Figure 1b), which is spectrally separate from the UV-range absorption peaks of fibrils and ThT<sup>15,16</sup>.

We investigated the molecular-scale mechanism behind the non-resonant changes in the chiroptical signals that are detected on the ensemble level (Figure 1a, SI Figure S1) and asked if these chiral signals can be attributed to either: (1) plasmon-coupled enhancement of differential absorption by the constricted ThT molecules near the AuNRs, or (2) templated aggregation of the AuNRs by the fibrils and ThT. We designed single-particle fluorescence polarimetry experiments to distinguish between these mechanisms by measuring if there is a significant chiroptical response when a single AuNR is coupled to fibrils and proximal to fibril-bound ThT molecules<sup>10</sup>. The experiments were also designed to investigate the heterogeneity in circular differential absorption of single particles, a distribution that is hidden in the ensemble measurement (Figure 1a). We find monomeric AuNRs have no detectable induced CD signal and thus, the net CD signal cannot be attributed to the sum of the induced CD from monomeric AuNRs. Furthermore, we find that small AuNR aggregates are not preferentially handed such

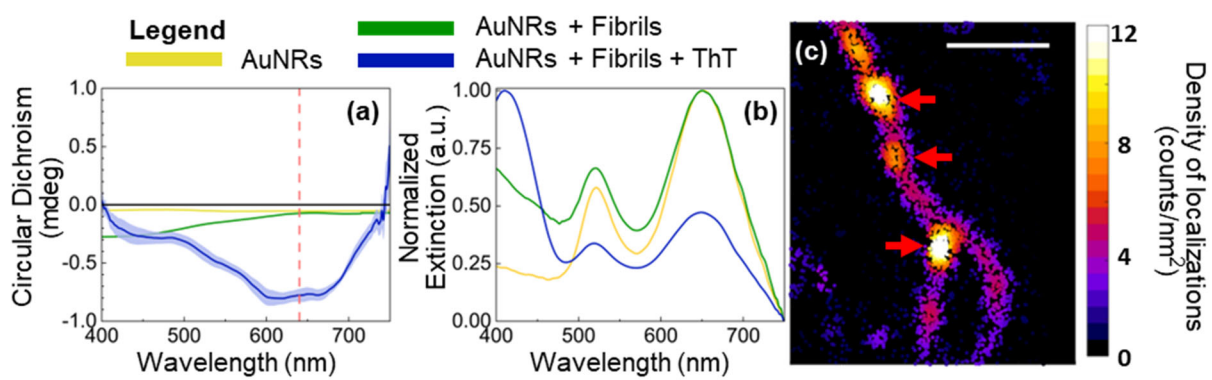


**Figure 1. Spectroscopic properties of AuNRs, fibrils, and ThT.** (a) Circular dichroism spectra and (b) normalized extinction spectra for solutions at pH 6. Red dotted line: 633-nm excitation wavelength for subsequent single-particle PL measurements. Light blue shading in panel ‘a’: standard deviation from five replicates. (c) Super-resolution image of ThT molecules adsorbed onto fibrils near AuNRs (red arrows) at 488-nm excitation. Scale bar: 1  $\mu$ m.

that the net CD signal cannot be attributed to the sum of CD from small aggregates. Thus, the net CD signal must be dominated by the CD signal from only a few non-representative AuNR aggregates. Our results point to the need for a high-throughput single-particle sampling detection scheme to attain a molecular-scale understanding given the heterogeneous distribution of CD response from AuNR aggregates in the presence of fibrils and ThT<sup>17</sup>.

We prepared insulin fibrils at pH 6 and mixed 100  $\mu$ L of the fibrils with 300  $\mu$ L of 80 nm  $\times$  40 nm AuNRs in 40  $\mu$ M of the blue intercalating dye ThT. When ThT is added to the solution of fibrils and AuNRs, there is an increase in dissymmetry around the AuNR plasmon resonance frequency of 640 nm based on ensemble circular dichroism (CD) and absorbance measurements (SI methods; Figure 1a-b). This change in absorbance at 640 nm upon the addition of a non-resonant dye is unexpected and particularly interesting because it allows us to study the coupling effects with negligible background from the dye molecules, which are much more blue: ThT molecules emit strongly upon excitation at 488 nm but are not detected upon excitation at 640 nm, whereas the AuNR PL is significant upon excitation at 640 nm.

Since only the AuNRs are optically active around 640 nm, this dissymmetry change is characterized as induced CD from the AuNRs. This increased dissymmetry has been seen in similar plasmonic nanoparticle/protein interactions<sup>18,19</sup>. In solution, several factors can lead to a net change in CD, thus, we took a single-particle approach to understand the changes in the absorption of single AuNRs with changes in the surrounding media. We implemented a polarization-sensitive single-molecule microscope to measure PL-detected CD from single emitters (SI Figure S2)<sup>10</sup>. We compensated for phase changes in the optical path (primarily due to multiple reflections and the dichroic filter) and alternated between left- and right-handed circularly polarized excitations with a variable waveplate (Thorlabs LCC1223T-A). The incident beam was left-handed circularly polarized when the phase between the orthogonal axes was +90° and right-handed circularly polarized when the phase between the orthogonal axes was -90°. After propagation through the convergent optics in the system, the polarization was optimized to circularity  $\geq$  95% for both handednesses in all experiments as monitored with a power meter at the sample stage using a linear polarizer mounted in a rotation mount. We used a wide-field epifluorescence microscope for imaging: the excitation beam was focused on the back aperture of the objective to achieve a collimated beam at the sample stage. This setup ensures uniform

polarization at the sample and also avoids any phase changes due to the high NA objective in the excitation pathway. First, we quantified how AuNRs affect the fluorescence of ThT bound to the fibrils. ThT is a fluorogenic dye that has an increased fluorescence quantum yield when bound to fibrils due to immobilization on these  $\beta$ -sheet structures. We detected the fluorescence pattern of each isolated ThT molecule as it transiently adsorbed to the fibril, used single-molecule localization to determine the apparent position of that molecule, and constructed a super-resolution map of the positions along the fibrils. (Figure 1c)<sup>14,20,21</sup>. We detected ThT molecules along the fibrils, thus confirming that AuNRs do not hinder the transient adsorption of ThT onto fibrils. There appears to be a higher density of ThT molecule localizations near the AuNRs (red arrows in Figure 1c), but this observation is consistent with expected mislocalization toward the plasmonic antenna in plasmon-coupled single-molecule measurements<sup>22-24</sup>. Moreover, under handed excitation, ThT fluorescence intensity does not significantly change, because the AuNRs do not have a strong optical response resonant to the dye.

We then used PL-detected CD measurements of single particles to probe if the induced CD measured at 640 nm by bulk spectroscopy is consistent with the sum of induced CD from a collection of monomeric AuNRs or if the net CD signal is dominated by a subset of AuNRs.

We compared the PL brightness (PL intensity normalized by the acquisition time) under left- and right-handed excitation over each diffraction-limited spot. The percentage difference in PL,  $\Delta PL$  (Figures 2 and 3) was calculated as:

$$\Delta PL = \frac{2(I_L - I_R)}{(I_L + I_R)} \times 100 \% \quad (1)$$

where  $I_L$  and  $I_R$  are the PL brightnesses upon left- and right-handed excitation, respectively. Because PL is directly proportional to absorbance, comparing the PL intensity of the particles (Figure 2a) under left- and right-handed excitation indicates their differential absorbance.

First, monomeric AuNRs were drop-cast onto a coverslip coated with poly-L-lysine. The coverslip was washed with water to remove excess AuNRs in solution and to ensure a good coverage of immobilized AuNRs. Monomeric AuNRs were identified using dark-field scattering spectroscopy<sup>25</sup> (SI Figure S3). The  $\Delta PL$  of the AuNRs in water was then measured and calculated (Figure 2b). The non-zero values of  $\Delta PL$  of the monomeric AuNRs account for the

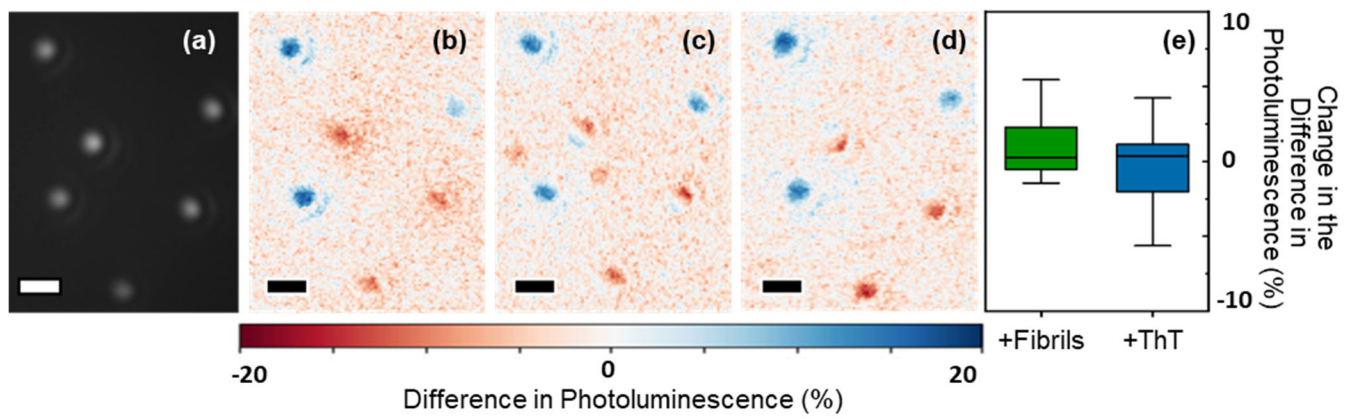


**Figure 2. No consistent change is measured for the differential photoluminescence (PL) of AuNRs in the vicinity of fibrils and ThT.** (a) Integrated PL image (excitation wavelength: 635 nm). (b – c) Plots of percentage difference of PL intensity between LCP and RCP excitation for the same field of view: (b) only AuNRs, (c) sample in ‘b’ after the addition and adsorption of fibrils, (d) sample in ‘c’ after the addition of 40  $\mu$ M ThT. Scale bars: 1  $\mu$ m. (e) Change in percentage difference in PL of AuNRs with the addition of fibrils (i.e., panel ‘c’ minus panel ‘b’) and ThT (i.e., panel ‘d’ minus panel ‘c’) for  $N = 18$  AuNRs. Box limits: 25 – 75% range; center lines: means; whiskers: data extrema.

low CD signal: even achiral AuNRs produce due to lattice asymmetries<sup>26</sup>. Artifacts due to linear dichroism are minimized by ensuring a  $\geq 95\%$  circularly polarized excitation and by sampling AuNRs at random orientations. An excess of fibrils was added to the AuNRs on the microscope coverslip and the fibrils were left to settle and stick to the slide for an hour before measuring the  $\Delta PL$  of the same AuNRs (Figure 2c). We then added an excess of ThT to the AuNRs and fibrils on the microscope coverslip. The ThT molecules adsorbed onto the fibrils immediately, so we measured the  $\Delta PL$  of the same AuNRs after adding ThT (Figure 2d).

If the bulk signal is consistent with the effects of single AuNRs, we would expect to see a decrease in the  $\Delta PL$  of the monomeric AuNRs (Figure 2b) after adding fibrils and ThT, because there is a strong dip in the ensemble CD signal at 640 nm (Figure 1a). However,  $\Delta PL$  does not change significantly when fibrils are added (Figure 2c), nor when ThT binds to the fibrils (Figure 2d). This characterization was performed for  $N = 18$  particles (Figure 2b-d; SI Figure S4). We observed no significant change in  $\Delta PL$  between the three conditions, and no consistent change was recorded among the particles (Figure 2e). Thus, we conclude that the net CD seen in the bulk measurement is not the sum of the induced CD from each monomeric AuNR.

Previous work has also shown that fibrils and small complexes favor the formation of AuNR aggregations that tend to be handed<sup>19,27</sup>. When mixed with fibrils, the 80 nm  $\times$  40 nm AuNRs in this experiment are observed in transmission electron microscopy (TEM) images to aggregate in a variety of configurations (Figure 3e), thus our second hypothesis was that the bulk CD signal is dominated by AuNRs that form small chiral aggregates with a favored handedness upon mixing with fibrils and ThT. This hypothesis is consistent with similar chiral templating that has been observed for other small proteins<sup>28-30</sup>. In earlier experiments, we avoided aggregation by sequentially adding components to focus on measuring the effect of nearby fibrils and ThT on the induced CD from monomeric AuNRs. Here, we instead formed agglomerates and characterized their handedness by mixing AuNRs in an Eppendorf tube either with a solution of only fibrils (Figure 3a-b) or with a solution of fibrils and ThT (Figure 3c-d). By mixing in a tube before drop-casting onto the coverslip, we allowed aggregates to form in solution; these aggregates were then immobilized onto a poly-L-lysine-coated coverslip. The coverslip was washed gently with Milli-Q water to remove any fibrils or AuNRs that were not immobilized. PL images were taken under left and right circularly polarized excitation for both these solutions

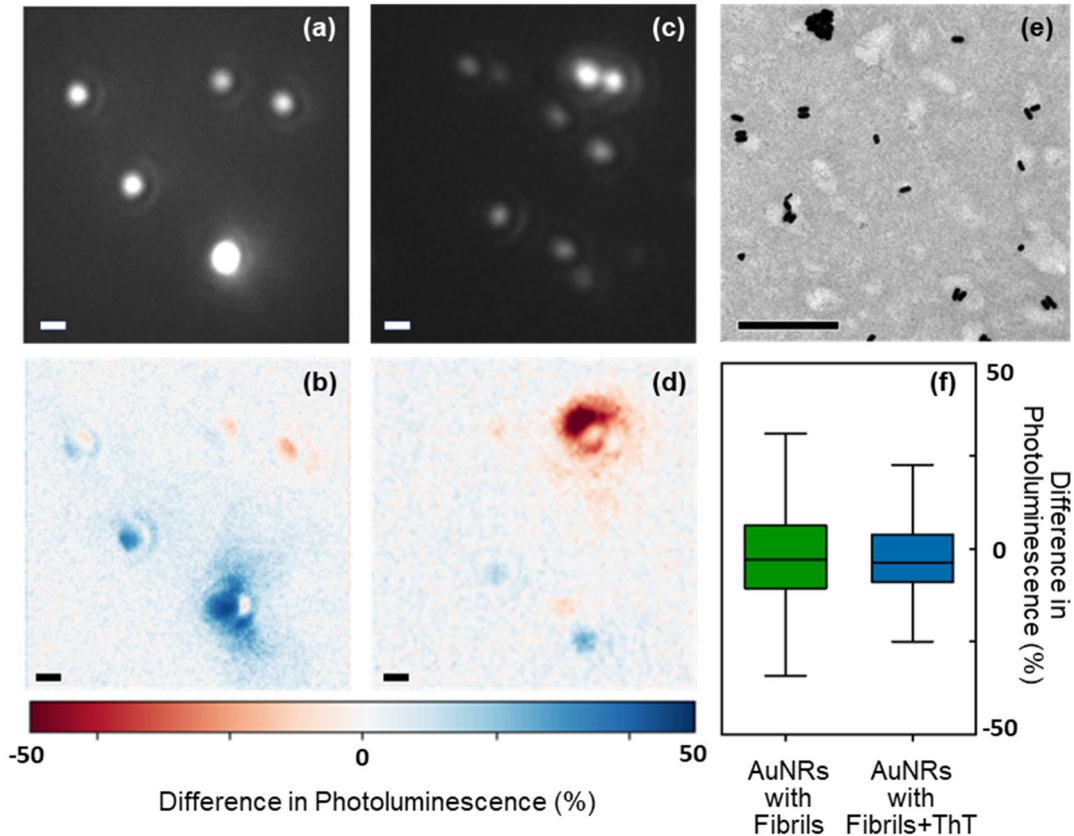


**Figure 3. AuNR aggregation upon mixing with fibrils and ThT in an Eppendorf tube at pH 6.** (a – b) AuNR aggregates in a fibril solution: (a) Integrated photoluminescence (PL) image (excitation wavelength: 635 nm). (b) Plot of percentage difference of PL intensity between LCP and RCP excitation for the same field of view. (c – d) AuNR aggregates in a fibril and ThT solution: (c) Integrated PL image (excitation wavelength: 635 nm). (d) Plot of percentage difference of PL intensity between LCP and RCP excitation for the same field of view. (e) TEM image of AuNR aggregates formed in a solution of fibrils and ThT at the same conditions. Scale bars: 1  $\mu$ m. (f) Percentage difference in PL intensity between LCP and RCP excitation of AuNR aggregates formed in solution with: fibrils at pH 6; or fibrils and ThT at pH 6 for  $N = 30$  aggregates. Box limits: 25 – 75% range; center lines: means; whiskers: data extrema.

(Figure 3a,c). The  $\Delta PL$  for each sample was calculated using Equation (1) (Figure 3b,d). We observed that these aggregates have much higher magnitudes of  $\Delta PL$ , and thus exhibit a higher CD response than the monomeric AuNRs in Figure 2, but they are not preferentially templated into right- or left-handed aggregates (Figure 3f); any observed bias is within our measurement error (SI Figure S5). From the ensemble CD measurement (Figure 1a), we had expected a skew towards more right-handed aggregates when the AuNRs were mixed with the fibrils and the ThT, but our single particle measurement suggests that the ThT does not play such a big role in the chirality of small aggregates, and in both solutions, the net effect of the small aggregates on the ensemble CD would thus be zero.

Since our experimental setup only captures the effect of fibrils and ThT on AuNR monomers (Figure 2) and small AuNR aggregates with diffraction-limited point spread functions immobilized on poly-L-lysine coated coverslips (Figure 3), our observations exclude any larger 3D chiral structures. Thus, our single-particle results indicate that the CD signal is dominated by the chiroptical response from only a subset of large AuNR aggregates and is not representative of the sum of the signals from monomeric AuNRs coupled to fibrils and constricted ThT molecule, nor to small aggregates of AuNRs.

In conclusion, we have designed and implemented a single-particle polarimeter sensitive to a 5% difference in PL to conclude that the introduction of an excess of intercalating dye is not enough to enable the detection of the chirality of fibrils at the single-particle level. There is no significant and consistent enhancement of differential absorption by the monomeric AuNRs due to ThT bound to nearby fibrils, and there is a heterogeneous distribution of handedness in the aggregates. The skew toward a specific fibril handedness is negligible for small aggregates. Additional aggregation factors, such as salt concentrations and pH, need to be explored before using these 80 nm  $\times$  40 nm gold nanorods to build single-particle chirality sensors. In addition to directly probing chirality in biological systems, the microscope setup can also be used to study the chiroptical properties of more elaborate substrates like chiral antenna arrays that can be deployed for sensing by redirecting the emission from molecules.

## **Supporting Information**

Supporting methods and figures detailing spectroscopic properties, single-particle polarimeter set-up, and PL intensity differences.

## **Conflict of Interest Disclosure**

The authors declare no competing financial interest.

## **Acknowledgements**

This work was supported by National Sciences Foundation grant CHE-1807676 to J.S.B., and J.O.-B. was supported by the Sonata Bis 9 project (2019/34/E/ST5/00276) financed by the National Science Centre in Poland.

## References

- (1) Dzwolak, W. Chirality and Chiroptical Properties of Amyloid Fibrils. *Chirality* **2014**, *26* (9), 580–587. DOI: 10.1002/chir.22335.
- (2) Dzwolak, W.; Pecul, M. Chiral Bias of Amyloid Fibrils Revealed by the Twisted Conformation of Thioflavin T: An Induced Circular Dichroism/DFT Study. *FEBS Lett.* **2005**, *579* (29), 6601–6603. DOI: 10.1016/j.febslet.2005.10.048.
- (3) Eisenberg, D.; Jucker, M. The Amyloid State of Proteins in Human Diseases. *Cell* **2012**, *148* (6), 1188–1203. DOI: 10.1016/j.cell.2012.02.022.
- (4) Chiti, F.; Dobson, C. M. Protein Misfolding, Amyloid Formation, and Human Disease: A Summary of Progress over the Last Decade. *Annu. Rev. Biochem.* **2017**, *86* (1), 27–68. DOI: 10.1146/annurev-biochem-061516-045115.
- (5) Louros, N.; Schymkowitz, J.; Rousseau, F. Mechanisms and Pathology of Protein Misfolding and Aggregation. *Nat. Rev. Mol. Cell Biol.* **2023**, 1–22. DOI: 10.1038/s41580-023-00647-2.
- (6) Stroo, E.; Koopman, M.; Nollen, E. A. A.; Mata-Cabana, A. Cellular Regulation of Amyloid Formation in Aging and Disease. *Front. Neurosci.* **2017**, *11*. DOI: 10.3389/fnins.2017.00064
- (7) Hartl, F. U. Protein Misfolding Diseases. *Annu. Rev. Biochem.* **2017**, *86* (1), 21–26. DOI: 10.1146/annurev-biochem-061516-044518.
- (8) Warerkar, O. D.; Mudliar, N. H.; Ahuja, T.; Shahane, S. D.; Singh, P. K. A Highly Sensitive Hemicyanine-Based Near-Infrared Fluorescence Sensor for Detecting Toxic Amyloid Aggregates in Human Serum. *Int. J. Biol. Macromol.* **2023**, *247*, 125621. DOI: 10.1016/j.ijbiomac.2023.125621.
- (9) Holman, A. P.; Quinn, K.; Kumar, R.; Kmiecik, S.; Ali, A.; Kurouski, D. Fatty Acids Reverse the Supramolecular Chirality of Insulin Fibrils. *J. Phys. Chem. Lett.* **2023**, *14* (30), 6935–6939. DOI: 10.1021/acs.jpcllett.3c01527.
- (10) Pfaffenberger, Z. J.; Chattopadhyay, S.; Biteen, J. S. Far-Field Polarization Optics Control the Nanometer-Scale Pattern of High-Fluorescence Dissymmetry Emission from Achiral Molecules near Plasmonic Nanodimers. *J. Phys. Chem. C* **2023**, *127* (20), 9663–9672. DOI: 10.1021/acs.jpcc.3c00467.
- (11) Kumar, J.; Eraña, H.; López-Martínez, E.; Claes, N.; Martín, V. F.; Solís, D. M.; Bals, S.; Cortajarena, A. L.; Castilla, J.; Liz-Marzán, L. M. Detection of Amyloid Fibrils in Parkinson’s Disease Using Plasmonic Chirality. *Proc. Natl. Acad. Sci.* **2018**, *115* (13), 3225–3230. DOI: 10.1073/pnas.1721690115.
- (12) Lan, X.; Zhou, X.; McCarthy, L. A.; Govorov, A. O.; Liu, Y.; Link, S. DNA-Enabled Chiral Gold Nanoparticle–Chromophore Hybrid Structure with Resonant Plasmon–Exciton

Coupling Gives Unusual and Strong Circular Dichroism. *J. Am. Chem. Soc.* **2019**, *141* (49), 19336–19341. DOI: 10.1021/jacs.9b08797.

(13) Rybicka, A.; Longhi, G.; Castiglioni, E.; Abbate, S.; Dzwolak, W.; Babenko, V.; Pecul, M. Thioflavin T: Electronic Circular Dichroism and Circularly Polarized Luminescence Induced by Amyloid Fibrils. *ChemPhysChem* **2016**, *17* (18), 2931–2937. DOI: 10.1002/cphc.201600235.

(14) Xue, C.; Lin, T. Y.; Chang, D.; Guo, Z. Thioflavin T as an Amyloid Dye: Fibril Quantification, Optimal Concentration and Effect on Aggregation. *R. Soc. Open Sci.* **2017**, *4* (1), 160696. DOI: 10.1098/rsos.160696.

(15) Iannuzzi, C.; Borriello, M.; Portaccio, M.; Irace, G.; Sirangelo, I. Insights into Insulin Fibril Assembly at Physiological and Acidic pH and Related Amyloid Intrinsic Fluorescence. *Int. J. Mol. Sci.* **2017**, *18* (12), 2551. DOI: 10.3390/ijms18122551.

(16) Johansson, P. K.; Koelsch, P. Label-Free Imaging of Amyloids Using Their Intrinsic Linear and Nonlinear Optical Properties. *Biomed. Opt. Express* **2017**, *8* (2), 743–756. DOI: 10.1364/BOE.8.000743.

(17) Sachs, J.; Günther, J.-P.; Mark, A. G.; Fischer, P. Chiroptical Spectroscopy of a Freely Diffusing Single Nanoparticle. *Nat. Commun.* **2020**, *11* (1), 4513. DOI: 10.1038/s41467-020-18166-5.

(18) Warning, L. A.; Miandashti, A. R.; Misiura, A.; Landes, C. F.; Link, S. Naturally Occurring Proteins Direct Chiral Nanorod Aggregation. *J. Phys. Chem. C* **2022**, *126* (5), 2656–2668. DOI: 10.1021/acs.jpcc.1c09644.

(19) Shinmori, H.; Mochizuki, C. Strong Chiroptical Activity from Achiral Gold Nanorods Assembled with Proteins. *Chem. Commun.* **2017**, *53* (49), 6569–6572. DOI: 10.1039/C7CC03089D.

(20) Isaacoff, B. P.; Li, Y.; Lee, S. A.; Biteen, J. S. SMALL-LABS: Measuring Single-Molecule Intensity and Position in Obscuring Backgrounds. *Biophys. J.* **2019**, *116* (6), 975–982. DOI: 10.1016/j.bpj.2019.02.006.

(21) Gade Malmos, K.; Blancas-Mejia, L. M.; Weber, B.; Buchner, J.; Ramirez-Alvarado, M.; Naiki, H.; Otzen, D. ThT 101: A Primer on the Use of Thioflavin T to Investigate Amyloid Formation. *Amyloid* **2017**, *24* (1), 1–16. DOI: 10.1080/13506129.2017.1304905.

(22) Goldwyn, H. J.; Smith, K. C.; Busche, J. A.; Masiello, D. J. Mislocalization in Plasmon-Enhanced Single-Molecule Fluorescence Microscopy as a Dynamical Young's Interferometer. *ACS Photonics* **2018**, *5* (8), 3141–3151. DOI: 10.1021/acsphotonics.8b00372.

(23) Wertz, E.; Isaacoff, B. P.; Flynn, J. D.; Biteen, J. S. Single-Molecule Super-Resolution Microscopy Reveals How Light Couples to a Plasmonic Nanoantenna on the Nanometer Scale. *Nano Lett.* **2015**, *15* (4), 2662–2670. DOI: 10.1021/acs.nanolett.5b00319.

(24) Willets, K. A.; Wilson, A. J.; Sundaresan, V.; Joshi, P. B. Super-Resolution Imaging and Plasmonics. *Chem. Rev.* **2017**, *117* (11), 7538–7582. DOI: 10.1021/acs.chemrev.6b00547.

(25) Hu, M.; Novo, C.; Funston, A.; Wang, H.; Staleva, H.; Zou, S.; Mulvaney, P.; Xia, Y.; V. Hartland, G. Dark-Field Microscopy Studies of Single Metal Nanoparticles: Understanding the Factors That Influence the Linewidth of the Localized Surface Plasmon Resonance. *J. Mater. Chem.* **2008**, *18* (17), 1949–1960. DOI: 10.1039/B714759G.

(26) Li, Z.; Kang, L.; Lord, R. W.; Park, K.; Gillman, A.; Vaia, R. A.; Schaak, R. E.; Werner, D. H.; Knappenberger, K. L. Jr. Plasmon-Mediated Chiroptical Second Harmonic Generation from Seemingly Achiral Gold Nanorods. *ACS Nanosci. Au* **2022**, *2* (1), 32–39. DOI: 10.1021/acsnanoscienceau.1c00014.

(27) Dominguez-Medina, S.; Kisley, L.; Tauzin, L. J.; Hoggard, A.; Shuang, B.; D. S. Indrasekara, A. S.; Chen, S.; Wang, L.-Y.; Derry, P. J.; Liopo, A.; Zubarev, E. R.; Landes, C. F.; Link, S. Adsorption and Unfolding of a Single Protein Triggers Nanoparticle Aggregation. *ACS Nano* **2016**, *10* (2), 2103–2112. DOI: 10.1021/acsnano.5b06439.

(28) Zhang, Q.; Hernandez, T.; Smith, K. W.; Hosseini Jebeli, S. A.; Dai, A. X.; Warning, L.; Baiyasi, R.; McCarthy, L. A.; Guo, H.; Chen, D.-H.; Dionne, J. A.; Landes, C. F.; Link, S. Unraveling the Origin of Chirality from Plasmonic Nanoparticle-Protein Complexes. *Science* **2019**, *365* (6460), 1475–1478. DOI: 10.1126/science.aax5415.

(29) Rose Thomas, A.; Swetha, K.; K, A. C.; Ashraf, R.; Kumar, J.; Kumar, S.; S. Mandal, S. Protein Fibril Assisted Chiral Assembly of Gold Nanorods. *J. Mater. Chem. B* **2022**, *10* (33), 6360–6371. DOI: 10.1039/D2TB01419J.

(30) George, J.; Thomas, K. G. Surface Plasmon Coupled Circular Dichroism of Au Nanoparticles on Peptide Nanotubes. *J. Am. Chem. Soc.* **2010**, *132* (8), 2502–2503. DOI: 10.1021/ja908574j.